J. Fluid Mech. (2012), *vol.* 703, *pp.* 315–325. © Cambridge University Press 2012
doi:10.1017/jfm.2012.218

Wicking of a liquid bridge connected to a moving porous surface

A. D. Gat[1]†, H. K. Navaz[2] and M. Gharib[1]

[1] Graduate Aerospace Laboratories, California Institute of Technology, Pasadena, CA 91125, USA

[2] Department of Mechanical Engineering, University of Kettering, Flint, MI 48504, USA

(Received 10 January 2012; revised 19 March 2012; accepted 2 May 2012;
first published online 12 June 2012)

We study the coupled problem of a liquid bridge connected to a porous surface and an impermeable surface, where the gap between the surfaces is an externally controlled function of time. The relative motion between the surfaces influences the pressure distribution and geometry of the liquid bridge, thus affecting the shape of liquid penetration into the porous material. Utilizing the lubrication approximation and Darcy's phenomenological law, we obtain an implicit integral relation between the relative motion between the surfaces and the shape of liquid penetration. A method to control the shape of liquid penetration is suggested and illustrated for the case of conical penetration shapes with an arbitrary cone opening angle. We obtain explicit analytic expressions for the case of constant relative speed of the surfaces as well as for the relative motion between the surfaces required to create conical penetration shapes. Our theoretical results are compared with experiments and reasonable agreement between the analytical and experimental data is observed.

Key words: capillary flows, liquid bridges, porous media

1. Introduction

We study a liquid bridge connecting a porous surface and an impermeable surface in order to obtain a relation between $h(t)$, the externally controlled time-varying gap between the surfaces, and the function $l(r, t)$, describing the depth of penetration into the porous material for radial coordinate r and time t (see figure 1). The relative motion between the surfaces affects the contact area between the liquid and the porous surface as well as the capillary and viscous forces, thus influencing the pressure distribution within the liquid bridge (Gat, Navaz & Gharib 2011). This, in turn, affects the rate of wicking and the liquid shape within the porous material (Darcy 1856; Washburn 1921).

By analysing the influence of the relative speed between the surfaces on the penetration shape of the liquid within the porous material, we obtain a control mechanism for the liquid penetration shape. This mechanism can be utilized in various applications. For example, by achieving constant penetration depth ($l(r, t) = \text{const.}$), it is possible to reduce the amount of liquid required in printing (Daniel & Berg 2006) or coating processes, as well as enabling a more efficient utilization of absorbing

† Email address for correspondence: amirgat@caltech.edu

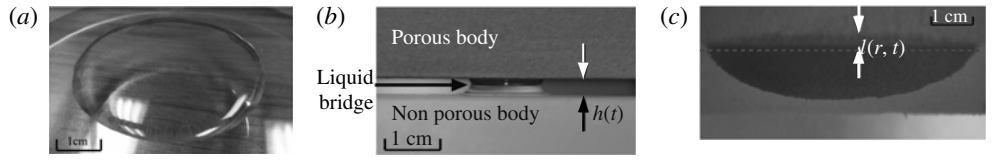

FIGURE 1. A porous surface (Oasis^{TM} Maxlife) is lowered and comes into contact with a glycerol droplet suspended on a fused silica plate (*a*). A liquid bridge connecting the porous and impermeable surfaces is created (*b*) and is absorbed into the porous material. After the wicking ended, we cut the permeable surface at the dashed line (*c*). We can thus observe a cross-section of the permeable material (above the dashed line) as well as the imprint of the liquid on the bottom surface of the porous material (below the dashed line). The wetted regions are darker compared with the dry regions.

materials in cleaning applications (e.g. removing oil droplets from a flat surface). Similarly, our model enables the prediction of the depth and radius of penetration of a contaminated droplet suspended on a flat surface and in contact with a moving porous material, which is relevant to the design of protection from chemical agents (Markicevic, D'Onofrio & Navaz 2010).

Liquid bridges connecting porous bodies have been studied in the context of flows through fractured porous media (Dindoruk & Firoozabadi 1994; Or & Ghezzehei 2007; Dejam & Hassanzadeh 2011). Similar problems involving coupled flow within and outside a porous medium have been analysed by various researchers, including Tilton & Cortelezzi (2008), who investigated the stability of flows in channels with porous walls, and Liu & Prosperetti (2011), who conducted a numerical study of finite-Reynolds-number pressure-driven flows through channels with porous walls, as well as others (e.g. Majdalani, Zhou & Dawson 2002; Dinarvand, Rashidi & Doosthoseini 2009). However, the most related and extensively studied problem is the primary penetration of a sessile droplet into a porous medium, where wicking into the porous surface is coupled to the volume of the droplet, the pressure within the droplet, and the contact area between the liquid and the porous surface (Davis & Hocking 1999; D'Onofrio *et al.* 2009; Markicevic *et al.* 2010, among others).

The rest of this paper is organized as follows: in § 2 we obtain an implicit integral relation between the relative motion of the surfaces and the penetration shape of the liquid. Section 3.1 presents solutions for several simplified cases of the obtained implicit integral relation. In § 3.2 a scheme for controlling the liquid penetration shape is presented and illustrated. In § 3.3 we present and compare our analytic results with experimental data. In § 4 we conclude and suggest future research directions.

2. Analysis

We study the wicking of a liquid bridge connecting a porous surface and an impermeable surface. The geometry and cylindrical coordinate system of the problem are defined in figure 2. The gap between the surfaces, denoted by the function $h(t)$, is time-varying and externally controlled. The flow between the surfaces is coupled to the flow within the porous material and to the gap and relative speed of the surfaces. We focus on axisymmetric creeping flows where the dominant balance of the governing equations, both within and outside the porous body, is between the viscous resistance of the liquid and the pressure gradient.

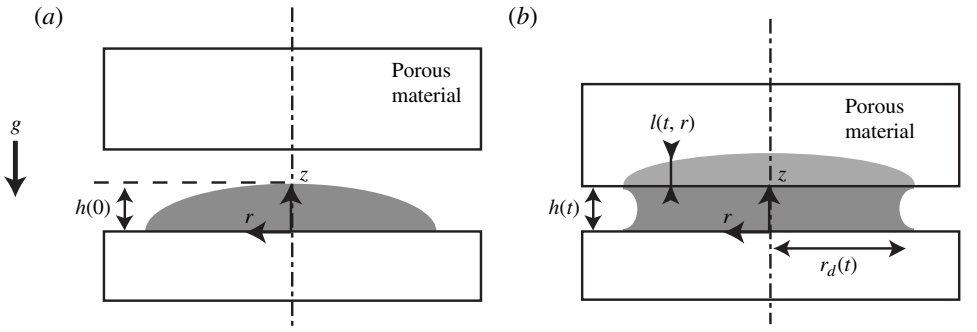

FIGURE 2. A schematic description of a liquid bridge connecting a moving porous surface and an impermeable surface (*a*) before and (*b*) after contact with the porous surface.

Assuming a Newtonian incompressible liquid, the axisymmetric flow between the surfaces (see figure 2) is governed by the Navier–Stokes equations

$$\rho\left(\frac{\partial u_r}{\partial t}+u_r\frac{\partial u_r}{\partial r}+u_z\frac{\partial u_r}{\partial z}\right)=-\frac{\partial p}{\partial r}+\mu\left[\frac{1}{r}\frac{\partial}{\partial r}\left(r\frac{\partial u_r}{\partial r}\right)+\frac{\partial^2 u_r}{\partial z^2}-\frac{u_r}{r^2}\right], \tag{2.1}$$

$$\rho\left(\frac{\partial u_z}{\partial t}+u_r\frac{\partial u_z}{\partial r}+u_z\frac{\partial u_z}{\partial z}\right)=-\frac{\partial p}{\partial z}+\mu\left[\frac{1}{r}\frac{\partial}{\partial r}\left(r\frac{\partial u_z}{\partial r}\right)+\frac{\partial^2 u_z}{\partial z^2}\right]+\rho g, \tag{2.2}$$

and conservation of mass

$$\frac{1}{r}\frac{\partial}{\partial r}\left(\frac{r}{u_r}\right)+\frac{\partial u_z}{\partial z}=0, \tag{2.3}$$

where t is time, ρ is density, μ is viscosity, g is gravity (acting in the z-direction), p is pressure, u_r and u_z are liquid speeds in the r and z directions, respectively.

The flow within the porous material is estimated from the phenomenological Darcy's law

$$\boldsymbol{q}=-\frac{\kappa}{\mu}\nabla p, \tag{2.4}$$

where κ is the permeability of the porous material and $\boldsymbol{q}$ is the Darcy flux vector.

The boundary conditions at the impermeable surface, $z=0$, are no-slip, $u_r=0$, and no-penetration, $u_z=0$. The relative speed between the surfaces is expressed within the model by the position of the liquid–porous surface boundary, $z=h(t)$, and the relevant boundary conditions of mass-flux conservation, $u_z=\partial h/\partial t+\phi\partial L/\partial t$ (ϕ is the porosity of the permeable material), and the slip velocity at $z=h(t)$. The liquid slip at $z=h(t)$ is proportional to $u_r(z=h(t))\propto\sqrt{\kappa}\partial u_r/\partial z$, where $\sqrt{\kappa}$ is the characteristic length scale of the permeable material (Beavers & Joseph 1967). The boundary condition at the gas–liquid interface is the dynamic stress balance (Leal 2007)

$$(\boldsymbol{\tau}^*-\boldsymbol{I}p^*)\cdot\hat{\boldsymbol{n}}-(\boldsymbol{\tau}-\boldsymbol{I}p)\cdot\hat{\boldsymbol{n}}+\gamma c\hat{\boldsymbol{n}}=0, \tag{2.5}$$

where p^* is the pressure of the surrounding gas, $\boldsymbol{\tau}^*$ is the stress tensor of the surrounding gas, $\boldsymbol{\tau}$ is the stress tensor of the liquid, γ is the surface tension, $\hat{\boldsymbol{n}}$ is a unit vector pointing outward from the liquid surface and c is the local curvature.

We require that the characteristic length scale in the z-direction, defined as $z_0=h(0)$ (see figure 2*a*), is much smaller than the characteristic length scale in the r-direction,

defined as $r_0 = \sqrt{V(0)/\pi z_0}$ (where $V(0)$ is the initial volume of the liquid bridge), and denote this ratio by

$$\varepsilon = \frac{z_0}{r_0} \ll 1. \tag{2.6}$$

As the liquid comes into contact with the upper porous surface, the liquid shape transforms from a sessile droplet (see figure 2*a*) into a liquid bridge (see figure 2*b*). The order of magnitude of time required for this transformation can be estimated from the r-direction momentum equation (2.1) as $O(r_0^2\mu/\gamma z_0)$ (neglecting inertia and estimating the capillary pressure as $\sim O(\gamma/z_0)$). We require that the time required to change the droplet shape into a liquid bridge is negligible in comparison with the characteristic time for liquid penetration into the porous material, $O(z_0^2\mu/\gamma\sqrt{\kappa})$ (obtained from order of magnitude analysis of the Darcy equation (2.4)), yielding the following limitation on the permeability:

$$\frac{\sqrt{\kappa}}{z_0} \ll \varepsilon^2. \tag{2.7}$$

Substituting the characteristic lengths into the continuity equation and performing order of magnitude analysis of (2.3), we obtain

$$\frac{w_0}{u_0} \sim \frac{z_0}{r_0} = \varepsilon, \tag{2.8}$$

where w_0 is the characteristic relative speed between the surfaces and u_0 is the characteristic liquid speed in the r-direction.

Hereafter, dimensionless variables are denoted by capital letters. We define the dimensionless coordinates $(R, Z) = (r/r_0, z/z_0)$, velocity $(U_r, U_z) = (u_r/u_0, u_z/w_0)$, time $T = tu_0/r_0$, gap $H = h/z_0$, liquid bridge radius $R_d = r_d/r_0$, penetration depth $L = l/z_0$, pressure $P = p/p_0$ (where p_0 is the characteristic pressure), curvature $C = z_0 c$, and liquid volume $V = v/z_0 r_0^2$. We denote $\varepsilon Re = \varepsilon\rho u_0 z_0/\mu$ as the reduced Reynolds number. For $\varepsilon Re \ll 1$, order of magnitude analysis of the r-direction conservation of momentum equation yields $p_0 = \mu u_0/\varepsilon^2 r_0$.

Substituting the normalized variables into the governing equations, the momentum conservation equations, to leading order, are reduced to

$$\frac{\partial P}{\partial R} = \frac{\partial^2 U_r}{\partial Z^2} + O(\varepsilon^2, \varepsilon Re) \tag{2.9}$$

and

$$\frac{\partial P}{\partial Z} = O\left(\varepsilon^2, \varepsilon Re, \frac{z_0 g\rho}{p_0}\right). \tag{2.10}$$

We require that the viscosity of the gas μ^* within and outside the porous medium is small in comparison with the viscosity of the penetrating liquid, $\mu^* \ll \mu$. Thus, the dynamics of the flow of the gaseous phase can be neglected. Normalizing the boundary conditions, the dynamic stress balance at the gas–liquid interface, to leading order, is reduced to

$$P - P^* + C\frac{\varepsilon^2}{C_a} \sim 0, \tag{2.11}$$

where $C_a = \mu v_0/\gamma$ is the capillary number and $P^* = p^*/p_0$. For $\varepsilon \to 0$ and under the above assumptions, the curvature at the liquid–gas interface is part of a circular

arc and can be estimated from geometric relations as (De Souza *et al.* 2008) $C \sim (\cos\theta_1 + \cos\theta_2)/H(T)$, where θ_1 and θ_2 are the static (advancing or receding) wetting angles at the upper and bottom surfaces, respectively. Thus, the pressure at the liquid–gas interface $R = R_d(Z, T)$ is given by

$$P(R = R_d) \sim P^* - \frac{\varepsilon^2}{C_a}\frac{\cos\theta_1 + \cos\theta_2}{H(T)}. \tag{2.12}$$

For the case of $C_a \sim \varepsilon^2$, the wetting angles will approach their static advancing or receding values (De Gennes, Brochard-Wyart & Quéré 2004; Sikalo, Tropea & Ganic 2005) and for the case of $C_a \gg \varepsilon^2$ the influence of surface tension is negligible and thus (2.12) is valid, to leading order, for any capillary number C_a. Utilizing (2.7), the slip at the liquid–porous surface boundary is $U(Z = H(T)) \sim O(\varepsilon^2)$ and is thus negligible. All other normalized boundary conditions remain unchanged.

The ratio between the pressure drop due to gravity, acting in the z-direction, and the characteristic pressure drop p_0 per length r_0 is assumed to be small, $z_0 g\rho/p_0 \ll 1$, and thus gravity can be neglected both between the two surfaces and within the porous material. Integration of the r-direction momentum equation (2.9) and the application of the no-slip boundary conditions on the upper and bottom surfaces yields

$$U_r \sim \frac{\partial P}{\partial R}\left(\frac{Z^2}{2} - \frac{H(T)Z}{2}\right). \tag{2.13}$$

We substitute U_r into the conservation of mass equation (2.3) and integrate from $Z = 0$ to $H(T)$ in order to obtain the relation

$$-\frac{H^3(T)}{12}\frac{1}{R}\frac{\partial}{\partial R}\left(R\frac{\partial P}{\partial R}\right) + \frac{\partial H(T)}{\partial T} \sim -\phi\frac{\partial L(R, T)}{\partial T}. \tag{2.14}$$

Defining $K = \kappa/\varepsilon^2 z_0^2$ as the dimensionless permeability and denoting the normalized pressure difference due to the capillary forces within the porous material by $P_c = p_c/p_0 \propto \gamma/\sqrt{\kappa}p_0$ (p_c, the dimensional capillary pressure within the porous material, can be estimated from porosimetry measurements, the average pore radius or wicking experiments), (2.4) is reduced, to leading order, to the relation

$$\frac{\partial L(R, T)}{\partial T} \sim K\frac{P(R, T) - P^* + P_c}{L(R, T)}. \tag{2.15}$$

The value of $R_d(Z, T)$ can be presented by integral conservation of mass as

$$R_d(Z, T) = \sqrt{\frac{V(0) - V_A(T)}{\pi H(T)}} + O(\varepsilon), \tag{2.16}$$

where $V(0)$ is the initial volume of the liquid bridge and $V_A(T)$ is the volume of fluid within the porous medium. While the $O(\varepsilon)$ terms at the right-hand side of (2.16) might be dependent on Z, the leading-order term is independent of Z and thus as $\varepsilon \to 0$, $R_d(Z, T) \to R_d(T)$.

The value of $V_A(T)$ (normalized by $z_0 r_0^2$) is defined by

$$V_A(T) = 2\pi\phi\int_0^{R_d(T)} RL(T, R)\,\mathrm{d}R. \tag{2.17}$$

Since $K = \kappa/\varepsilon^2 z_0^2 \ll 1$ (see (2.7)), the right-hand side term in (2.14) can be neglected in the leading order. Equation (2.14) can thus be integrated with regard to R and by

applying symmetry conditions at $R = 0$ and boundary condition (2.12) at $R \sim R_d(T)$, we obtain

$$P(R,T) - P^* \sim \left(R^2 - \frac{V(0) - V_A(T)}{\pi H(T)} \right) \frac{\partial H(T)}{\partial T} \frac{3}{H^3(T)} - \frac{\varepsilon^2}{C_a} \frac{\cos\theta_1 + \cos\theta_2}{H(T)}. \quad (2.18)$$

Integrating (2.15), while utilizing (2.16) to assess the area of the porous surface in contact with the liquid bridge, yields

$$L^2(R,T) - L^2(R,0) \sim 2K \int_0^T (P(R,\eta) - P^* + P_c) \times H_S \left(\sqrt{\frac{V(0) - V_A(\eta)}{\pi H(\eta)}} - R \right) \mathrm{d}\eta, \quad (2.19)$$

where H_S is the Heaviside function. Substituting (2.18) and (2.19) into (2.17), we thus relate the pressure field within the liquid bridge to the rate of wicking into the porous material, eliminate the function $L(R,T)$ and obtain an implicit integral equation for the absorbed liquid volume $V_A(T)$:

$$V_A(T) \sim 2\phi\pi \int_0^\infty \left\{ R \sqrt{ \int_0^T \left[\begin{array}{l} 2KH_S \left(\dfrac{V(0) - V_A(\eta)}{\pi H(\eta)} - R^2 \right) \times \\ \left(\left(R^2 - \dfrac{V(0) - V_A(\eta)}{\pi H(\eta)} \right) \dfrac{\partial H(\eta)}{\partial T} \dfrac{3}{H^3(\eta)} \right. \\ \left. - \varepsilon^2 \dfrac{\cos(\theta_1) + \cos(\theta_2)}{C_a H(\eta)} + P_c \right) \\ + L^2(R,0) \end{array} \right] \mathrm{d}\eta } \right\} \mathrm{d}R. \quad (2.20)$$

Hence, for a general function $H(T)$, (2.20) can be solved to obtain $V_A(T)$, which in turn allows for the calculation of $L(R,T)$ by (2.18) and (2.19).

3. Results

3.1. *Simplified solutions*

Obtaining an analytic solution of the implicit integral relation (2.20) is not possible for all cases. However, for the initial stages of liquid penetration, $V_A(T)/V(0) \ll 1$, (2.20) can be readily simplified and an explicit solution for $V_A(T)$ can be calculated. Furthermore, analytic integration of (2.20) is possible for cases such as $P_c \gg 1$, $\varepsilon^2 C_a^{-1}$ and $H(T) = H(0) + W_s T$, where $W_s = w_s/w_0$ is the speed of the permeable surface. Under the above limitations, the expression describing $V_A(t)$ can be simplified to

$$V_A(T) \sim \phi V(0) \sqrt{\frac{2KP_c}{W_s H(T)}} \ln \left(\sqrt{\frac{H(T)}{H(0)}} + \sqrt{\frac{H(T)}{H(0)} - 1} \right). \quad (3.1)$$

A numerical scheme for solving the implicit integral equation (2.20) can be obtained by expanding the right-hand side terms to Taylor series around $T = T_0$. This expansion yields a relation between the $\partial V(T_0)/\partial T$ and $V(T_0)$ enabling direct numerical integration with regard to time of $V(T_0)$:

$$\frac{\partial V(T_0)}{\partial T} \sim 2\phi\pi K \int_0^{R_d(T_0)} \frac{P(R,T_0) - P^* + P_c}{L(R,T_0)} R \, \mathrm{d}R, \quad (3.2)$$

which, in combination with (2.19) and (2.18), allows for a rapid numerical solution of the problem.

3.2. *A scheme to control the topology of liquid penetration*

The obtained relation between the penetration profile of the liquid into the porous medium, $L(R, T)$, and the time-varying gap between the surfaces, $H(T)$, can be utilized as a controlling mechanism for determining $L(R, T)$. Defining the required (axisymmetric) penetration shape by $F(R) = L(T \to \infty, R)$ (normalized by z_0), the functions $R_d(T)$ and $V_A(T)$ can be calculated from (2.19) and (2.20). This, in turn, allows the calculation of the function $H(T)$ required to achieve the desired penetration shape. The range of penetration profiles $F(R)$ which can be created by this scheme depends on the physical coefficients P_c and C_a. For $P_c \ll 1$, which is physically the most common case, all penetration profiles $F(R)$ will monotonically decrease with R, for any function $H(T)$. For general penetration shape $F(R)$, this method may be applied utilizing iterative numerical methods. However, for simple penetration geometries and $P_c \gg 1$, analytic solution of the problem may be possible.

We illustrate this scheme for the case of a conical penetration profile with half-opening angle α and assuming $P_c \gg 1$ (an appropriate assumption for many physical configurations). We define $F(R) = (R_d(0) - R)/\varepsilon \tan\alpha$ and require $L(R_d(T), T \to \infty) = F(R)$. We calculate $R_d(T)$ from (2.19) as

$$R_d(T) \sim R_d(0) - \varepsilon\sqrt{2KP_cT}\tan\alpha, \tag{3.3}$$

and from (2.20) the value of $V_A(T)$ can be computed as

$$V_A(T) \sim 2\pi\phi\left[\sqrt{2KP_cT}\frac{R_d^2(T)}{2} - \left(\frac{R_d^2(T)R_d(0)}{2} - \frac{R_d^3(0)}{6} - \frac{R_d^3(T)}{3}\right)\frac{1}{\varepsilon\tan\alpha}\right]. \tag{3.4}$$

After calculating $V_A(T)$ and $R_d(T)$, the relative motion between the surfaces required to create a conical penetration profile is readily obtained from $H(T) \sim (V(0) - V_A(T))/\pi R_d^2(T)$.

We note that if the initial volume of the liquid bridge is smaller than the available void volume within the conical shape, only part of the cone shape will be wetted (see figure 5). No solution is possible if the initial volume of the liquid bridge is greater than the available void volume.

3.3. *Comparison with experiments*

In this section we present our analytical results and compare the analytic and experimental data.

We designed and constructed an experimental setup consisting of a linear stage actuator (Thorlabs™ LNR50SEK1) controlling the distance between two parallel surfaces, a fused silica optical window used as the impermeable surface, and a porous glass (Vykor™ 7930) or alternatively a plastic foam (Oasis™ Maxlife) used as the porous surface (see figure 1). The liquids used in the experiments are glycerol and deionized (DI) water and in all examined cases $P_c \gg 1, \varepsilon^2/C_a$, and thus the influence of the capillary effects on the pressure distribution within the liquid bridge can be neglected.

Figure 3 presents a comparison between experimental and theoretical data of the volume (*a*) and radius (*b*) versus time of a liquid bridge connecting an impermeable surface and a porous surface moving at a constant speed. The porous material used is Vykor™ 7930 porous glass with porosity of $\phi = 0.28$ and permeability

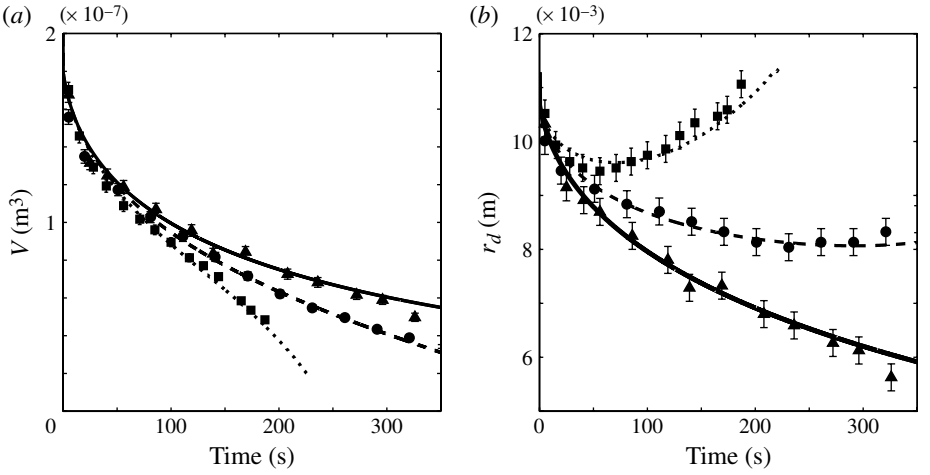

FIGURE 3. Comparison of experimental and theoretical data of liquid bridge volume (a) and radius (b) versus time. The initial gap between the surface is $h(0) = 5 \times 10^{-4}$ m, the porous material is Vykor™ 7930, and the liquid is a 2×10^{-7} m^3 DI water. Data for $\partial h/\partial t = 0$, -10^{-6} and -2×10^{-6} m s^{-1} are presented by solid, dashed and dotted lines, respectively (analytic model), and triangle, circle and square symbols, respectively (experimental results).

of $\kappa = 2.08 \times 10^{-19}$ m^2. The pressure difference within the porous material due to capillary effects is $p_c = 3.6 \times 10^7$ Pa. The liquid used is a 2×10^{-7} m^3 DI water ($\mu = 10^{-3}$ Pa s, $\rho = 10^3$ kg m^{-3} and $\gamma = 0.072$ N m^{-1}) and the initial gap between the surfaces is $h(0) = 5 \times 10^{-4}$ m. Data for $\partial h/\partial t = 0$, -10^{-6} and -2×10^{-6} m s^{-1} are presented by solid, dashed and dotted lines, respectively (analytic model), and triangle, circle and square symbols, respectively (experimental results).

From figure 3(a) we observe that the time required for wicking of the liquid bridges decreases as the relative speed between the surfaces increases. From figure 3(b) we observe that the radius of the liquid bridges increases with the relative speed and a minimum of the radius is evident for $\partial h/\partial t = -2 \times 10^{-6}$ m s^{-1}, describing a transition from an initial stage of liquid bridge radius decreasing with time, to a later stage of liquid bridge radius increasing with time.

In figures 4 and 5 we present a comparison of the experimental and analytical penetration shapes. The porous material is Oasis™ Maxlife foam and the liquid is glycerol ($\mu = 1.41$ Pa s, $\rho = 1261$ kg m^{-3} and $\gamma = 0.064$ N m^{-1}). We examined constant relative speeds of $\partial h/\partial t = -2 \times 10^{-6}$, -4×10^{-6} and -8×10^{-6} m s^{-1} (figure 4) as well as the speed profile obtained by the suggested scheme to control the penetration shape (for the case of conical penetration with half-opening angles of $\alpha = 82$, 80 and 5°: see § 3.2 and figure 5). In all cases the initial gap is $h(0) = 1.5 \times 10^{-3}$ m and the liquid volume is 5×10^{-6} m^3. The porosity of the Oasis™ Maxlife foam was obtained from dry and wet weight measurements of identical volumes and is estimated to be $\phi = 0.96$. From measurements of wicking depth versus time, the value of the foam permeability is estimated as $\kappa = 6.6 \times 10^{-12}$ m^2 and, from capillary rise measurements, the pressure difference due to the capillary forces within the porous material is estimated as $p_c = 384$ Pa. The analytical shapes of liquid penetration are presented by white dotted lines and are superimposed over pictures of the cross-section of the porous material after the

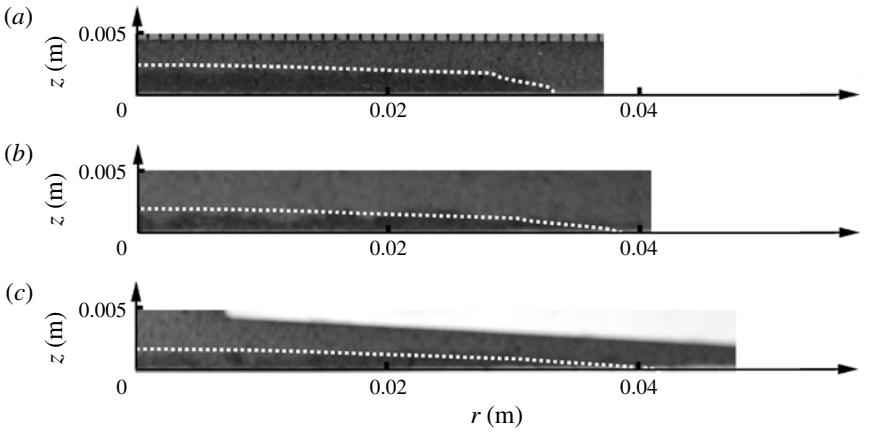

FIGURE 4. Experimental (dark regions) and theoretical (dotted lines) penetration shapes of a liquid bridge connecting a porous surface (Oasis^{TM} Maxlife) and a fused silica plate. The initial gap between the surfaces is $h(0) = 1.5 \times 10^{-3}$ m and (*a*) $\partial h/\partial t = -2 \times 10^{-6}$, (*b*) -4×10^{-6} and (*c*) -8×10^{-6} m s^{-1}. The liquid is glycerol and the volume is $V(0) = 5 \times 10^{-6}$ m^3.

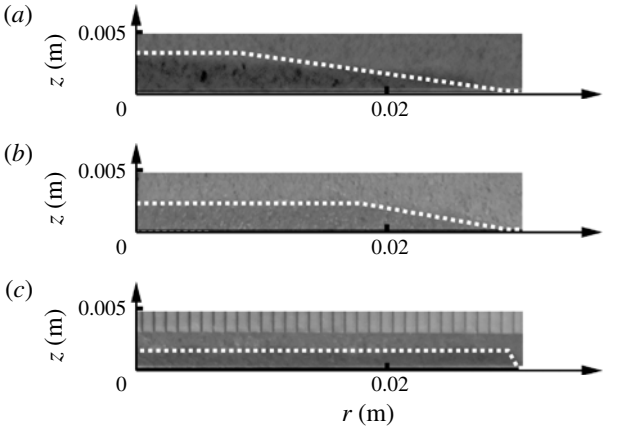

FIGURE 5. Experimental (dark regions) and theoretical (dotted lines) penetration shapes of a liquid bridge connecting a porous surface (Oasis^{TM} Maxlife) and a fused silica plate. The initial gap between the surfaces is defined by $h(0) = 1.5 \times 10^{-3}$ m and the speed profile $h(t)$ is obtained from the suggested scheme (see § 3.2) to control the penetration shape and create conical penetration shapes with half-opening angles of (*a*) $\alpha = 82^0$, (*b*) 80° and (*c*) 5°. The liquid is glycerol and the volume is $V(0) = 5 \times 10^{-6}$ m^3.

experiment (see figure 1*c*). The regions in which the liquid penetrated the porous material are darker compared to the dry regions and thus a visual comparison between the analytic solution and the experimental results can be made.

From figure 4 an increase in the maximal radius of the liquid bridge is observed as the relative speed increases. The maximal penetration depth of the liquid into the porous material decreases as the relative speed between the surfaces increases. For all examined cases reasonable agreement between the experimental and analytical

results is observed. Figure 5 presents partially wetted conical penetration shapes, where the limiting factor is the initial volume of the liquid bridge. As predicted, the function $h(t)$ obtained from § 3.2 significantly modifies the penetration shapes, compared with figure 4, and good agreement between the analytical and experimental data is observed.

4. Concluding remarks

By solving the coupled problem of Darcy's flow within the porous material and lubrication flow between the surfaces, we obtain a relation (2.20) between the function $H(T)$, describing the gap between the surfaces, and the volume of liquid within the porous material $V_A(T)$. After computing $V_A(T)$ the shape of liquid penetration into the porous material $L(R, T)$ can be calculated from (2.18) and (2.19). This relation is utilized within a scheme to control the penetration shape by controlling $H(T)$. The range of possible liquid penetration shapes is limited and dependent on the coefficients P_c and C_a. For many common configurations the dominant term is the capillary pressure, $P_c \gg 1$, which limits the penetration shape $F(R)$ to monotonically decreasing functions with regard to R.

The radial imprint of the liquid within the porous material is determined by the maximal value of the liquid bridge radius. For any value of $\partial H/\partial T$, the initial value of $\partial R_d/\partial T$ is negative. If the relative speed of the surfaces is small compared with the characteristic rate of liquid penetration, $\partial H/\partial T \ll P_c K$ (estimated from (2.15) and assuming $P_c \gg 1$), the liquid bridge radius will continue to decrease for the entire time required for the wicking of the liquid bridge. However, as $\partial H/\partial T$ increases and reaches an order of $O(P_c K)$ threshold speed, a minimum of the liquid bridge radius is created, after which the liquid bridge radius increases and may become greater than the initial radius (see figures 3 and 4). For $P_c \gg 1$ the radius of penetration monotonically increases with the relative speed and the average penetration depth decreases, suggesting that fast relative motion of the surfaces ($\partial H/\partial T \gg P_c K$) can be utilized to decrease the depth of liquid penetration into porous bodies.

The present study focused on motion perpendicular to the planes of the parallel surfaces. However, future research regarding tangential relative motion of the two surfaces can significantly increase the possible penetration shapes and allow for the creation of more complex and non-axisymmetric penetration profiles. Analysis of penetration of liquid bridges into saturated porous materials, and porous bodies with spatially varying permeability, is also of interest for future research, specifically in the context of the study of liquid penetration into skin.

Acknowledgement

We thank Dr S. Paikoff of the Defense Threat Reduction Agency (DTRA) which supported this project.

REFERENCES

BEAVERS, G. S. & JOSEPH, D. D. 1967 Boundary conditions at a naturally permeable wall. *J. Fluid Mech.* **30**, 197–207.

DANIEL, R. C. & BERG, J. C. 2006 Spreading on and penetration into thin, permeable print media: application to ink-jet printing. *Adv. Colloid Interface Sci.* **123–126**, 439–469.

DARCY, H. 1856 *Les Fontaines Publiques de la Ville de Dijon*. Dalmont.

DAVIS, S. H. & HOCKING, L. M. 1999 Spreading and imbibition of viscous liquid on a porous base. *Phys. Fluids* **11** (1), 48–57.

DE GENNES, P. G., BROCHARD-WYART, F. & QUÉRÉ, 2004 *Capillarity and Wetting Phenomena: Drops, Bubbles, Pearls, Waves*. Springer.

DE SOUZA, E. J., BRINKMANN, M., MOHRDIECK, C., CROSBY, A. & ARZT, E. 2008 Capillary forces between chemically different substrates. *Langmuir* **24**, 10161.

DEJAM, M. & HASSANZADEH, H. 2011 Formation of liquid bridges between porous matrix blocks. *AIChE J.* **57** (2), 286–298.

DINARVAND, S., RASHIDI, M. M. & DOOSTHOSEINI, A. 2009 Analytical approximate solutions for two-dimensional viscous flow through expanding or contracting gaps with permeable walls. *Cent. Euro. J. Physics* **7** (4), 791–799.

DINDORUK, B. & FIROOZABADI, A. 1994 Liquid film flow in a fracture between two porous blocks. *Phys. Fluids* **6** (12), 3861.

D'ONOFRIO, T. G., NAVAZ, H. K., MARKICEVIC, B, MANTOOTH, B. A. & SUMPTER, K. B. 2009 Experimental and numerical study of spread and sorption of VX sessile droplets into medium grain-size sand. *Langmuir* **26** (5), 3317–3322.

GAT, A. D., NAVAZ, H. & GHARIB, M. 2011 Dynamics of freely moving plates connected by a shallow liquid bridge. *Phys. Fluids* **23** (9), 097101.

LEAL, G. 2007 *Advanced Transport Phenomena: Fluid Mechanics and Convective Transport Processes*. Cambridge University Press.

LIU, Q. & PROSPERETTI, A. 2011 Pressure-driven flow in a channel with porous walls. *J. Fluid Mech.* **679**, 77–100.

MAJDALANI, J., ZHOU, C. & DAWSON, C. A. 2002 Two-dimensional viscous flow between slowly expanding or contracting walls with weak permeability. *J. Biomech.* **35** (10), 1399–1403.

MARKICEVIC, B., D'ONOFRIO, T. G. & NAVAZ, H. K. 2010 On spread extent of sessile droplet into porous medium: numerical solution and comparisons with experiments. *Phys. Fluids* **22** (1), 012103.

OR, D. & GHEZZEHEI, T. A. 2007 Traveling liquid bridges in unsaturated fractured porous media. *Trans. Porous Med.* **68** (1), 129–151.

SIKALO, S., TROPEA, C. & GANIC, E. 2005 Dynamic wetting angle of a spreading droplet. *Exp. Therm. Fluid Sci.* **29**, 795.

TILTON, N. & CORTELEZZI, L. 2008 Linear stability analysis of pressure-driven flows in channels with porous walls. *J. Fluid Mech.* **604**, 411–445.

WASHBURN, E. W. 1921 The dynamics of capillary flow. *Phys. Rev. Online Archive (Prola)* **17** (3), 273–283.